Chapter 14
LEAP-2017 Centrifuge Test at Ehime University

Mitsu Okamura and Asri Nurani Sjafruddin

Abstract Three centrifuge tests were conducted at Ehime University for the LEAP-2017 exercise. The experiment consisted of a submerged clean sand, with target relative densities of either 65 or 80%, with a 5 degree slope in a rigid container. Models were prepared along with the specifications and each model was subjected to a 1 Hz ramped sine wave base motion twice. This paper provides overview of the models and some details of the effects on the pore pressure responses of relative density and shaking histories of the models. Typical residual deformation obtained by PIV analysis and liquefaction resistance estimated based on the model response and laboratory cyclic shear tests are also shown.

14.1 Introduction

This paper presents three centrifuge tests conducted at Ehime University (EU) in the LEAP-2017 project. Model configuration, preparation techniques, and sand used are in accordance with "LEAP UCD 2017 VERSION 1.01 MODEL SPECIFICATIONS" (Kutter et al. 2018) otherwise mentioned. In this paper, a brief description of facilities at Ehime University to perform the tests and general information of the models are described first, followed by typical responses of the models.

14.2 Centrifuge at Ehime University

The centrifuge at EU has symmetrical rotor arms with swing platforms at each end. The radius at the top of the platform from the centrifuge axis is 1.25 m when the platforms fully swing up. In this study, an electronic mechanical shaker was used to

M. Okamura (✉)
Department of Science and Engineering, Ehime University, Matsuyama, Japan
e-mail: okamura@cee.ehime-u.ac.jp

A. N. Sjafruddin
Department of Civil Engineering, Ehime University, Matsuyama, Japan

B. Kutter et al. (eds.), *Model Tests and Numerical Simulations of Liquefaction and Lateral Spreading*, https://doi.org/10.1007/978-3-030-22818-7_14

impart simulated input motions to the models. A 0.6 kW AC inverter motor drives the shaking table horizontally through a camshaft of an eccentricity 0.7 mm. Horizontal displacement amplitude was approximately 0.7 mm and acceleration was controlled by rotation rate of the driving motor in the range between 0 and 50 Hz.

Data acquisition system equipped on the rotation arm allows to measure 48 sensors. All the signals are converted on board and sent through wireless USB connection to the PC in the laboratory.

14.3 Centrifuge Model

14.3.1 Model Description

A rigid model container was used with internal dimensions of 50 cm long, 12 cm wide, and 23 cm deep. Three models were prepared with target relative densities of either 65 or 80%, all saturated with 40 cSt viscous fluid and tested at 40 g with an exception that the second shaking for model 1 (EU1) was conducted at 20 g. Figure 14.1 shows a side view of the models. All the corresponding prototype dimensions are the same as those specified with an exception that the prototype width of 4.8 m was about a half that specified.

14.3.2 Sand

Ottawa F-65 sand was used in all the experiments, which was shipped out from UC Davis on March 2017. Sieve tests on the sand confirmed that grain size distributions

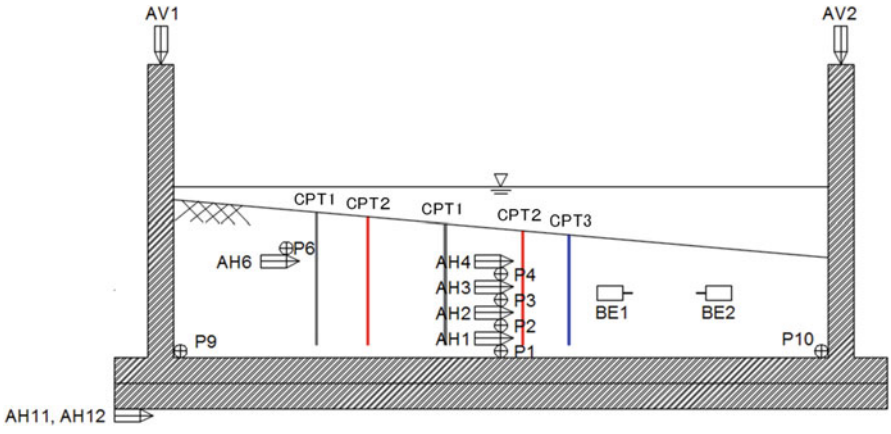

Fig. 14.1 Schematic of models

Table 14.1 Sieve test result

	This study	Specifications
D_{10} (mm)	0.113	0.133
D_{30} (mm)	0.171	0.173
D_{40} (mm)	0.248	0.203
D_{60} (mm)	0.265	0.215

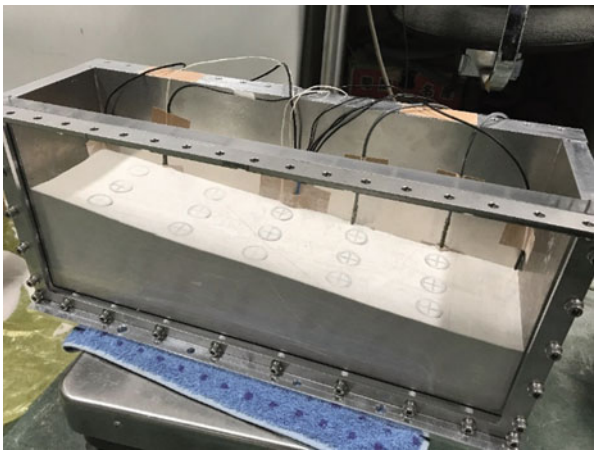

Fig. 14.2 Model before saturation

of the sand used in EU were consistent with those shown in the specifications (Table 14.1).

14.3.3 Placement of Sand

Dry sand stored in an air-conditioned room, and thus humidity was kept low, was pluviated into the container through a screen with an opening size 1.0 mm, rather than 1.2 mm specified in the specification, because openings of the standard sieve in JIS (Japanese Industrial Standard) is slightly different from ASTM.

Three arrangements of the screen masked off were used to achieve different target relative densities. 12 mm slots spaced at 25 or 7 mm slots spaced at 25 mm were used for preparing sand bed with relative density of 65% or 80%, respectively. After the pluviation of the sand, the surface of the model was leveled using a vacuum device to measure the height of model surface to calculate dry density. The procedure of the measuring height was the same as that specified. The surface was sloped using the vacuum device to 5 degrees and 18 surface markers were set (Fig. 14.2).

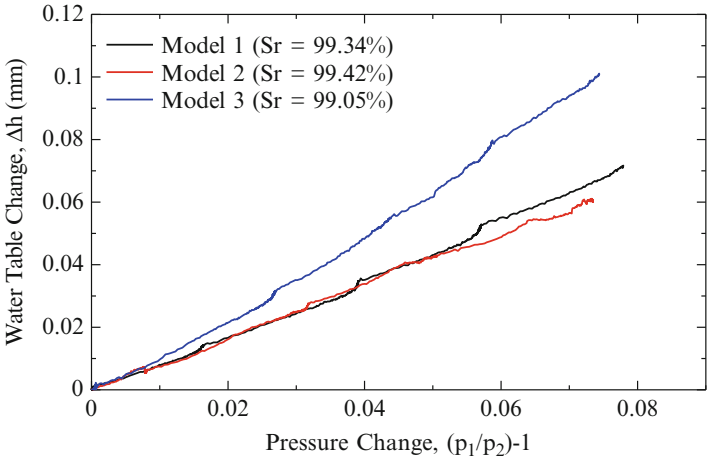

Fig. 14.3 Relationship between pressure in the chamber and change in water level

14.3.4 Saturation

The model container was moved into a vacuum chamber and the air in the chamber was replaced by CO_2. This was achieved by introducing vacuum pressure of −95 kPa and flooding CO_2 gas. De-aired viscous fluid was dripped into the low end of the model slope while keeping the vacuum of −95 kPa constant in the chamber and a fluid supply tank (Okamura and Inoue 2012). The viscous fluid was a mixture of water and hydroxypropyl methylcellulose (type 60SH-50) termed Metolose from Shin-Etsu Chemical Company (Shin-etsu Chemical Co. Ltd. 1997). This Metolose solution was prepared by dissolving 1.8% Metolose by weight in water, so as to achieve a viscosity of 40 times that of water (40 cSt kinematic viscosity). The viscosity of the fluid in each model was measured at room temperature before and after the tests with a rotational viscometer. The measured viscosity was in a range between 39 and 44 cSt.

On completion of the saturation process, the vacuum in the chamber was released and the model was rested in the atmospheric pressure for a few hours. A small change in the pressure of approximately 10 kPa was applied to the chamber at a constant rate approximately 5 kPa/min, and water level was measured with a LED displacement transducer with the resolution of 10 μm. Figure 14.3 indicates relationship between change in water level, Δh, and change in pressure (p1/p2 -1) observed for the three models, where p2 and p1 are the atmospheric pressure (101.3 kPa) and the pressure in the chamber, respectively (in absolute pressure). In each test linear relationships were observed. The degree of saturation of the models was estimated from the slope of the relationship (Okamura and Inoue 2012) and summarized in Table 14.2. The degree of saturation was in a range between 99.1 and 99.4%. In the centrifuge, hydrostatic pressure of the model was enhanced and most

Table 14.2 Relative density and degree of saturation of the models

Test code	Target D_r (%)	Before motion #1		Before motion #2	After motion #2
		D_r (%)	Degree of saturation, S_r (%)	D_r (%)	D_r (%)
EU1	65	64	99.3	71	80
EU2	65	67	99.4	77	79
EU3	80	83	99.1	87	88

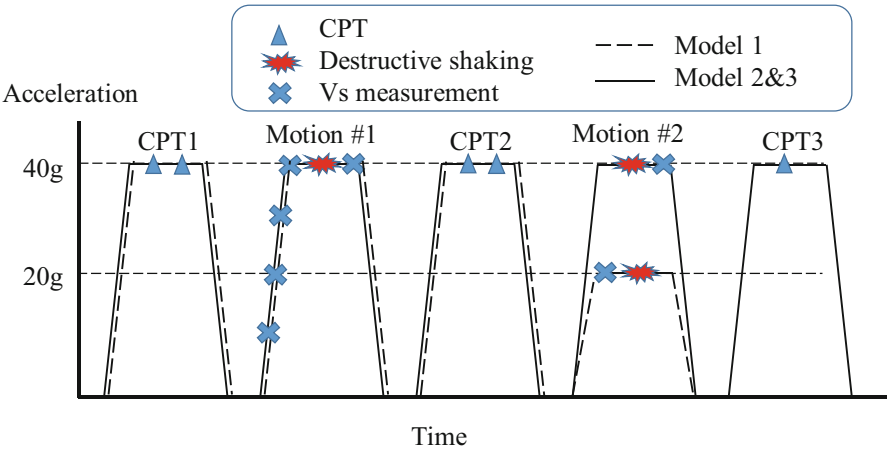

Fig. 14.4 Centrifuge test sequence

of the remaining air and CO_2 bubbles in soil pore are considered to have dissolved (Kutter 2013), which increased further the degree of saturation.

14.3.5 Test Procedure

Three tests were conducted in this study. Models EU1 and EU2 had the same relative density of approximately 65%, subjected to the same input motion. EU2 is the duplicate of EU1 to confirm reproducibility of test. Model EU3 had higher relative density of 85% and subjected to the same input motion as EU1 and EU2 to study effects of initial relative density of the models.

All shaking tests and CPT were carried out at 40 g except for the second shaking of model 1. The centrifuge was spun up and down to mount and unmount the CPT device as indicated in Fig. 14.4. Locations of the surface markers were measured with a ruler and relative density of the model was estimated from the average settlement which is summarized in Table 14.2.

Cone penetration tests were performed before and after every destructive ground motion with a CPT device designed and fabricated at UCD. Two penetration tests were conducted at a time at intervals of 5 cm (12.5 times the cone diameter). The rate of cone penetration was 0.6 mm/s in model scale, which was slower than that specified.

Horizontally travelling shear wave velocity was measured with a pair of bender elements installed at mid-depth in the model layers before and after every destructive ground motion. The bender elements of 12 mm × 7 mm in area were fix to acrylic blocks and set in the sand at a distance of 50 mm (tip to tip).

Two destructive shaking tests, Motion #1 and #2, were conducted for all the models. Motion #1 was the tapered sine wave with a maximum prototype acceleration amplitude of 0.15 g. In the second destructive shaking tests, the same motion as the first one was imparted again to evaluate the evolution of the behavior of the model due to the previous shaking event.

All the data was recorded at a sampling rate of 2000 per second during shaking and after shaking for approximately 20 s until generated pore pressure completely dissipated. In the subsequent section in this paper, all the test results are in prototype scale otherwise mentioned. Note that data were not applied any numerical filtering.

14.4 Results

14.4.1 Shear Wave Velocity

Shear wave velocities (V_s) measured with the bender elements at the mid-depth in EU1 and EU3 are indicated in Fig. 14.5. The measurement was performed before Motion #1, at 10 g, 20 g, 30 g, and 40 g, and velocities are plotted versus effective vertical stress at the depth of the bender element. V_s increased with increasing effective vertical stress, with V_s of EU3 being larger than EU1 because of the higher relative density.

14.4.2 Input Acceleration

Accelerometers fixed to the base of the container measured input acceleration and a typical record is shown in Fig. 14.6a together with the specified motion. In order to duplicate the specified tapered sine wave by the mechanical shaker, rotation rate of camshaft changed with time accordingly. The shaking initiated at the time $t = 0$ and the rotation rate increased linearly with time until $t = 10$ s and decreased thereafter. Therefore, the acceleration frequency was very close to 1.0 Hz for $t = 9$–11 s and between 0.7 and 0.9 Hz for $t = 5$–9 s and $t = 11$–15 s. Fourier spectrum of the input acceleration (AH11) is shown in Fig. 14.6b.

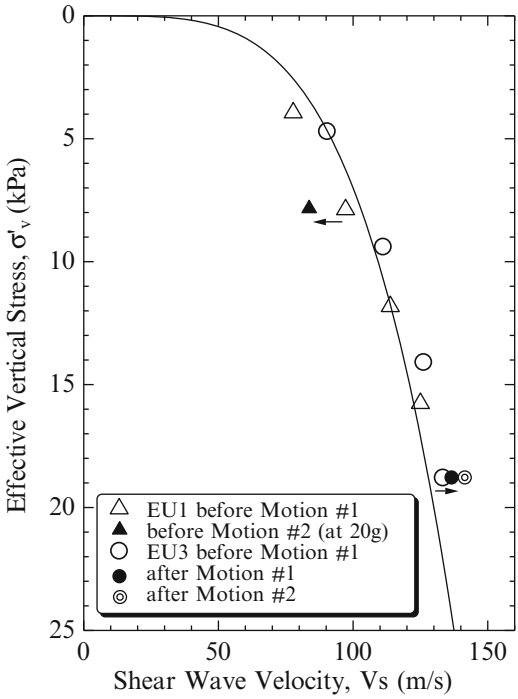

Fig. 14.5 Shear wave velocity

14.4.3 Excess Pore Pressure Response

1. Excess pore pressure ratio
   Figure 14.7 shows excess pore pressure ratios (EPPR) measured on the centerline of the models for the Motion #1 shaking events. EPPR reached unity except for p1, and EPPR of p1 was higher than 0.8, indicating that the soils in all the models liquefied from the surface to the depth close to the bottom. Comparison of EU1 and EU2 shows that EPPRs are very similar to each other in terms of maximum EPPR and time duration for liquefaction condition lasted after shaking ended. For EU3, with higher relative density than EU1 and EU2, EPPR of p2, p3, and p4 also reached unity, which was the same as the two models, but duration for liquefaction condition lasted after shaking ended was clearly shorter.
2. Reproducibility of test
   Figure 14.8 compares excess pore pressure (EPP) responses for Motion #1 of EU1 and EU2. The target relative density of these models was the same and EU2 was replication test of EU1. The input accelerations were quite similar in these tests. EPP was similar at all the depths except for p1 installed on the base of the container, showing a good reproducibility of the tests.
3. Effect of initial relative density

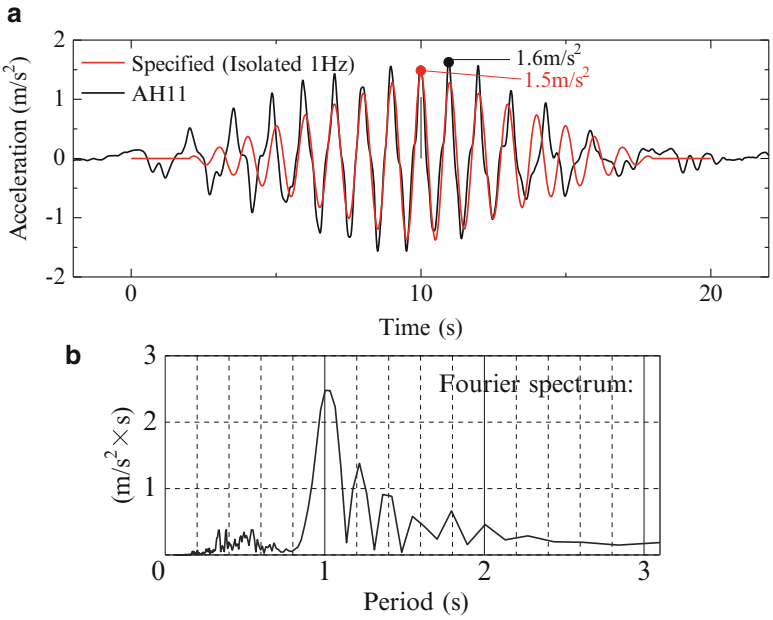

Fig. 14.6 Input acceleration of Motion #1 for EU1. (**a**) Acceleration recorded on the shaking table. (**b**) Fourier spectrum of input acceleration

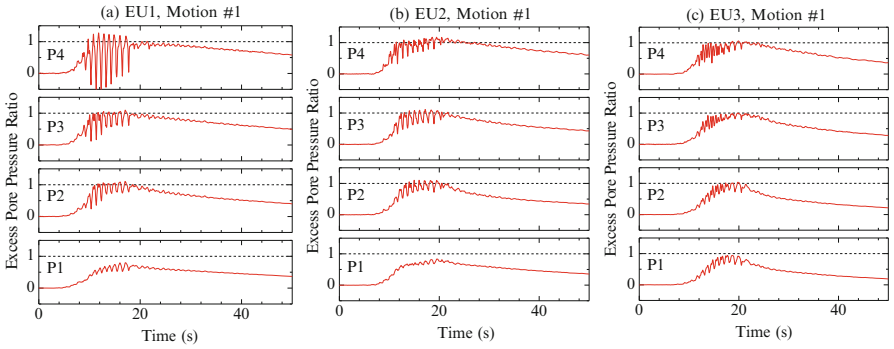

Fig. 14.7 Time histories of excess pore pressure ratio

Figure 14.9 compares EPP response of models with different initial density, EU2 ($D_r = 65\%$) and EU3 ($D_r = 80\%$) for Motion #1. Maximum excess pore pressure attained at depths was quite similar for the two models; however, the rate of the pore pressure generation was clearly different. For all the depths, EPP of EU2 reached liquefaction condition 1–2 s earlier than EU3. Shear wave velocity and cone tip resistance (q_t) were consistent with this. V_s and q_t of the model before Motion #1 were higher for EU3 ($D_r = 85\%$) than EU1 and EU2 ($D_r = 65\%$).

4. Effect of shaking history

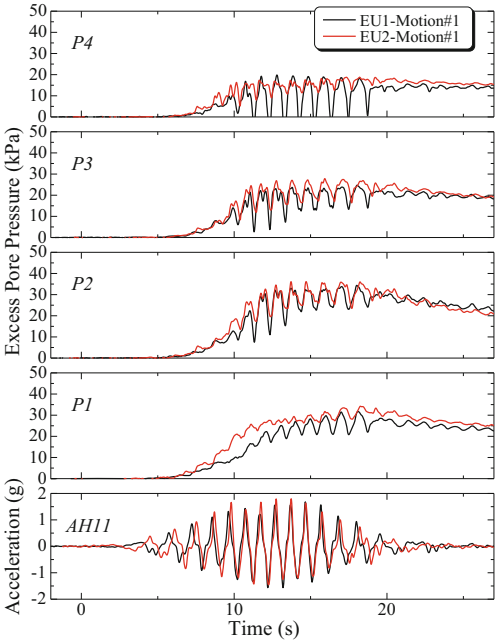

Fig. 14.8 Excess pore pressure response for Motion #1 of EU1 and EU2

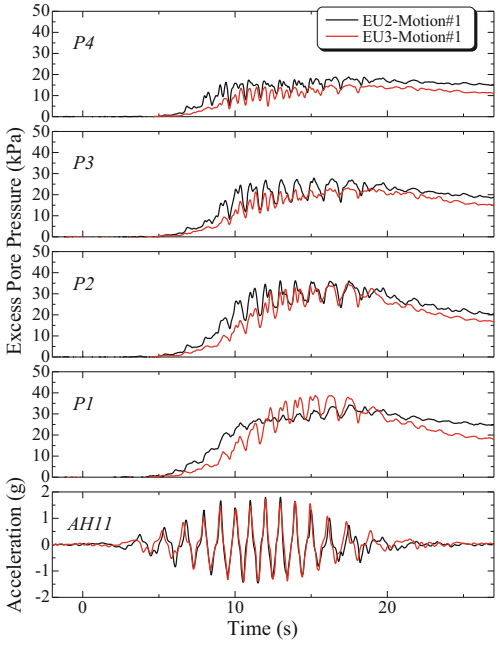

Fig. 14.9 Excess pore pressure response for Motion #1 of EU2 and EU3

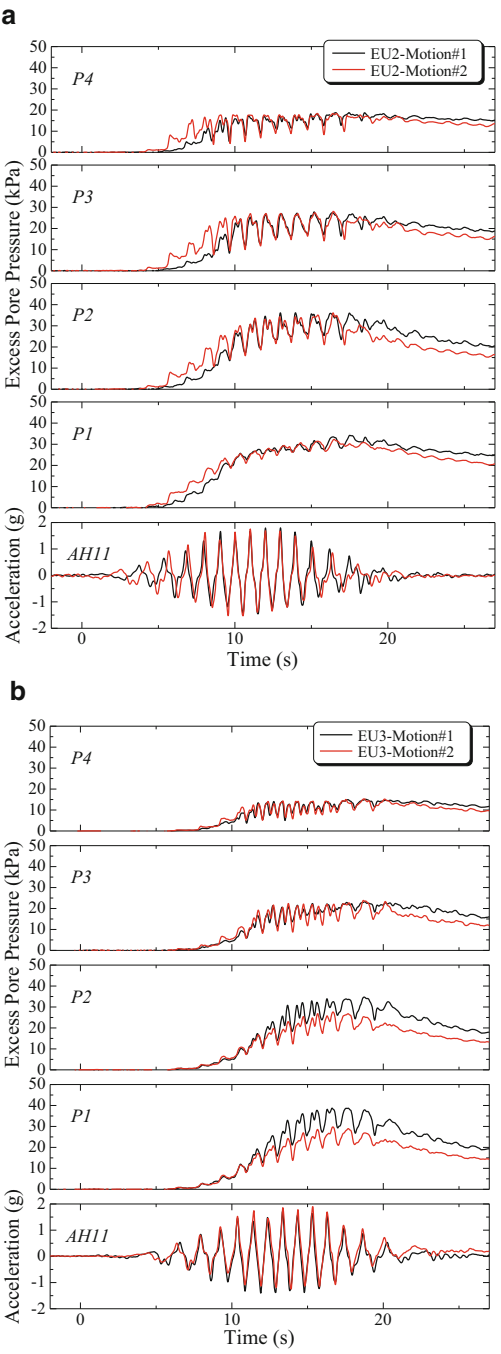

Fig. 14.10 Excess pore pressure response to Motions #1 and #2. (**a**) Model 2. (**b**) Model 3

EU2 and EU3 were subjected to the same input acceleration as Motions #1 and #2. Comparisons of the model responses to Motions #1 and #2 reveal the effect of the first shaking event (Motion #1) on the responses to the second shaking. Figure 14.10a shows such direct comparisons for EU2. Relative density of EU2 before Motion #1 was 67% and 77% before second event. Despite the increased relative density due to Motion #1, EPP for Motion #2 generated faster than Motion #1. The sand after first shaking was more prone to generate excess pore pressures. It is also noticed that q_c of EU2 after the first shaking event was very close to or slightly lower than that before first shaking event. Smaller V_s was observed after Motion #1.

EPP response for EU3 is compared in the same manner in Fig. 14.10b. Relative density of EU3 before first shaking event was 83% and 87% before second event. At shallower depth recorded EPP at p3 and p4 before and after Motion #1 practically coincided. At p2, EPP for Motions #1 and #2 also coincided until input acceleration reached its maximum at $t = 12.5$ s. Thereafter, EPP for Motion #1 kept high until $t = 20$ s while EPP for Motion #2 started to decrease. The first shaking had no effect on EPP response of the sand with $D_r = 80\%$ or slightly enhanced the resistance to cyclic pore pressure generation. V_s increased from 127 m/s before Motion #1 to 136 m/s before Motion #2 and further increased to 141 m/s after Motion #2 (see Fig. 14.5).

14.4.4 Liquefaction Triggering

In this study, an attempt was made to estimate liquefaction resistance of each model from model responses of Motion #1. Recorded acceleration was used to estimate cyclic shear stress ratio (CSR) at a depth of p3 assuming one-dimensional soil column condition. Because of the different number of cycles to liquefy in each test and nonuniform nature of CSR of each cycle as indicated in Fig. 14.11, the

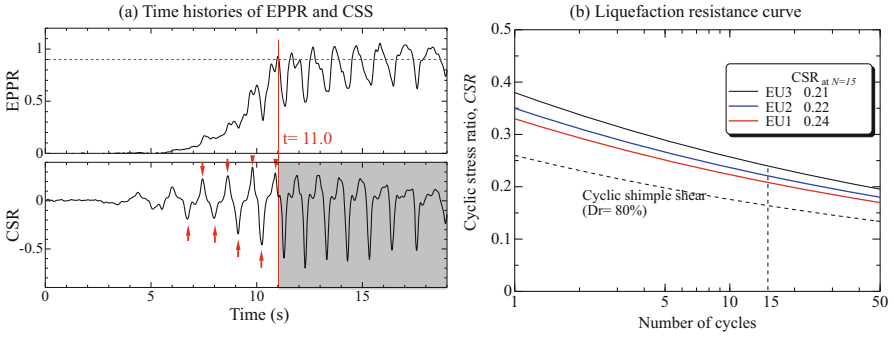

Fig. 14.11 CSR time histories of EU2 for Motion #1 and liquefaction resistance curves

cumulative damage theory was used. Results of undrained cyclic simple shear test on the sand (Bastidas et al. 2017), of which test conditions were similar to those of the centrifuge tests including the sand deposition method and relative density (40 and 80%), indicated that the liquefaction resistance curves can be approximated as:

$$\mathrm{CSR} = a \cdot N^{-0.15} \text{ for the sand with } D_\mathrm{r} = 40\% \tag{14.1}$$

and

$$\mathrm{CSR} = b \cdot N^{-0.17} \text{ for } D_\mathrm{r} = 80\% \tag{14.2}$$

where CSR is cyclic stress ratio to reach the liquefaction condition in N uniform cycles and a and b are constants. Since test results for relative density of 65% were not given and the exponents in these equations are close to each other, Eq. (14.2) was used to determine the coefficients b and thus cyclic resistance ratio of the centrifuge models.

Figure 14.11a shows typical time histories of excess pore pressure ratio and cyclic stress ratio at a depth 2 m from the surface. Based on the EPPR the soil is judged liquefied at $t = 11.0$ s (criteria is EPPR = 0.9). The peak values of CSR before this moment, shown by red triangles in Fig. 14.11a, were employed to calculate the cumulative damage.

Figure 14.11b shows relationship between CSR and number of cycles obtained from the simple shear test and those estimated for the centrifuge models for Motion #1. Liquefaction resistance ratio (CRR), which is defined in this study as the cyclic stress ratio to cause liquefaction condition in 15 uniform cycles, for EU1 and EU2 are depicted in Fig. 14.11b. CRR of EU1 and EU2 are similar and considerably lower than that for EU3, as expected. It is also noticed that CRR of the models are higher than the simple shear test result. A possible reason for this is existence of initial shear stress due to the sloping surface of the models. When the initial shear stress exists, the effective stress path can reach the failure line earlier which causes large acceleration spikes to the soil. The large acceleration spikes make the CSR significantly large. The other possible reasons are the use of the rigid container rather than a flexible laminar box and small vibrations which might have happened during model preparation.

14.4.5 Deformation of the Model

Side views of EU2 before and after Motion #1 in-flight are shown in Fig. 14.12. These pictures were taken with a USB3.0 camera with 5 megapixels at a frame rate of 30 Hz. Note that the width of the pictures is 12 m, while the model width is 20 m; therefore, areas near both side walls are not included. Particle image velocimetry analysis was conducted using the pictures and obtained deformation vectors are

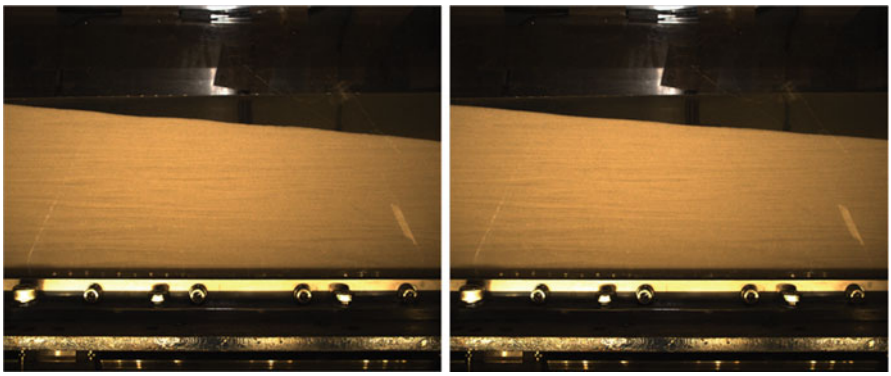

Fig. 14.12 Photos of EU2 before and after Motion #1

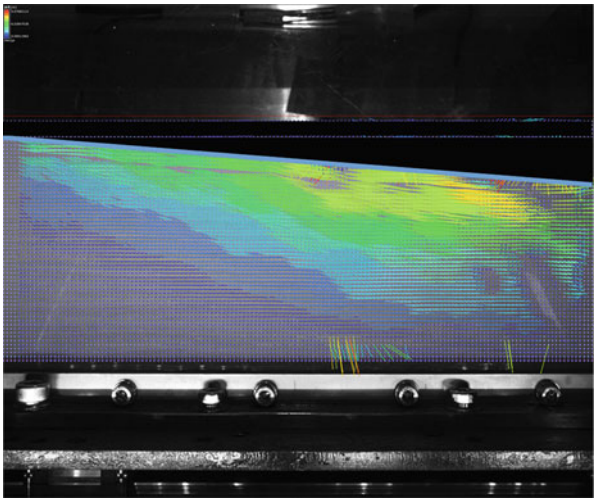

Fig. 14.13 Deformation vectors caused by Motion #1 of EU2

presented in Fig. 14.13. It can be seen that the movement of the soil was not uniform; soil at the upper right moved largely (yellow area), while displacement was limited in the lower left (dark blue area).

14.5 Conclusion

This paper describes three centrifuge tests conducted at Ehime University for LEAP-2017. The tested models were fully saturated uniform sand slope with relative density of either 65 or 80%. All the models were subjected the same ramped sine wave twice except for Motion #2 of EU2. The mechanical shaker was used to shake the models. The middle part of the input motion where the acceleration amplitude is largest had 1 Hz frequency, while the earlier and later part of the input motion had frequency lower than 1 Hz. Despite this nonconformity from the specification, input acceleration time histories of all shaking event for three models matched very closely. This makes it easy to study reproducibility of tests and effects of initial relative density, shaking history.

The same test was repeated in EU1 and EU2; the excess pore pressure responses of the two tests were quite similar, confirming intra-laboratory reproducibility. Destructive shaking and occurrence of liquefaction makes the medium dense sand (EU1 and EU2) more prone to generate excess pore pressure in the following shaking event. Shear wave velocity and cone tip resistance are also degraded by the destructive shaking. However, this is not the case for dense sand model (EU3) where pore pressure responses for Motions #1 and #2 practically coincided, and shear wave velocity increased from one shaking event to another.

An attempt was made to estimate liquefaction resistance of each model from model responses for Motion #1. Recorded acceleration was used to estimate cyclic shear stress ratio (CSR) assuming one-dimensional soil column condition, and the cumulative damage theory was used to account for the irregular nature of CSR time histories. The estimated liquefaction resistance of models are higher than those obtained from cyclic simple shear tests.

The distribution of the deformations in the model is analyzed with PIV. The displacement vectors are useful to obtain a broad view of entire deformation patterns.

Acknowledgments The experimental work was supported by JSPS KAKENHI Grant Number 26282103 (PI: Prof. S. Iai) and 17H00846 (PI: Prof. T. Tobita). The authors would like to thank a technical staff Mr. R. Tamaoka and students in the geotechnical group of EU T. Inoue, N. Sahashi, and S. Kubouchi for their assistance.

References

Bastidas, A. M. P., Boulanger, R. W., Carey, T. C., & DeJong, J. (2017). *Ottawa F-65 Sand Data from Ana Maria Parra Bastidas*. Retrieved from https://datacenterhub.org/resources/ottawa_f_65, https://doi.org/10.1002/glia.23161

Kutter, B. L. (2013). Effects of capillary number, bond number, and gas solubility on water saturation of sand specimens. *Canadian Geotechnical Journal, 50*(2), 133–144. https://doi.org/10.1139/cgj-2011-0250.

Kutter, B. L., Carey, T. J., Stone, N., Bonab, M. H., Manzari, M., Zeghal, M., Escoffier, S., Haigh, S., Madabhushi, G., Hung, W.-Y., Kim, D.-S., Kim, N.-R., Okamura, M., Tobita, T., Ueda, K., & Zhou, Y.-G. (2019). LEAP-UCD-2017 V. 1.01 model specifications. In B. Kutter et al. (Eds.), *Model tests and numerical simulations of liquefaction and lateral spreading: LEAP-UCD-2017*. New York: Springer. https://doi.org/10.1016/j.neuron.2018.08.036.

Okamura, M., & Inoue, T. (2012). Preparation of fully saturated model for liquefaction study. *International Journal of Physical Modelling in Geotechnics, 12*(1), 39–46. https://doi.org/10.1680/ijpmg.2012.12.1.39.

Shin-etsu Chemical Co., Ltd. (1997). *Metolose Brochure*. Cellulose Department, DOI: https://doi.org/10.17226/5702.